Capturing shock waves in inelastic granular gases

Susana Serna
Applied Mathematics, University of Valencia, Spain
e-mail susana.serna@uv.es
Antonio Marquina
Applied Mathematics, University of Valencia, Spain
e-mail marquina@uv.es

20 January 2004

Abstract

Shock waves in granular gases generated by either a vertically vibrated granular layer or by hitting an obstacle at rest are treated by means of a shock capturing scheme that approximates the Euler equations of granular gas dynamics with an equation of state (EOS), introduced by Goldshtein and Shapiro [J. Fluid Mech. 282 (1995) 75], that takes into account the inelastic collisions of granules. We include a sink term in the energy balance to account for dissipation of the granular motion by collisional inelasticity, proposed by Haff [J. Fluid Mech. 134 (1983) 401], and the gravity field added as source terms. We have implemented an approximate Riemann solver, due to the second author [J. Comput. Phys. 125 (1996) 42], that works robust under low granular temperatures, high Mach numbers and near close-packed limit, damping post-shock oscillations. We have performed several numerical tests to show numerical evidence of the above features. We have computed the approximate solution to the following problems: a one-dimensional granular gas falling on a plate under the acceleration of gravity until close-packed limit, various one-dimensional blast waves evolving in time in the absence of gravity, a one-dimensional vertically vibrated granular layer under a sinusoidal perturbation and the two-dimensional reflecting shock wave generated when granular gas hits an angular obstacule through the acceleration of gravity.

1 Introduction

Many experimental and theoretical work has been performed to study the fluid properties of granular gases. Several kinetic models were introduced to explain the complicated physical behavior of granular media. Shock waves are one of the difficult features appearing in fluidized granular gases and easily observed in laboratory, since typical speeds of sound of some granular gases are measured in cm/s. Hydrodynamical models are the most convenient and efficient ones to describe shock waves.

Research supported by DGICYT project BFM2001-2814 and ONR N00014-03-1-0071.

In this research work we are interested in simulating numerically shock wave dynamics using the Euler equations for a compressible granular flow described by means of a granular equation of state, (EOS), to compute the pressure, proposed by Goldshtein and Shapiro [7], that includes both dense gas and inelastic effects. We shall use an energy loss term, proportional to the $T^{\frac{3}{2}}$ being T the granular temperature, [11] that takes into account the inelastic collisions of particles. We also consider the possible effect of the acceleration of gravity added as source terms in both, the momentum equation and the energy equation. The above hydrodynamic model was designed to describe the fluid-like properties of granular flows of a vibrated bed, and it should be able to take into account the physical mechanism responsible for the transformation of the kinetic energy applied on the vibrating bed into granular temperature. This hydrodynamic model might be considered the resulting investigation of many researchers along the years, [1, 2, 7, 8, 9, 10, 11, 12, 13, 15, 22, 23].

In this paper, we use an approximate Riemann solver, written in the form of the so-called Marquina's Flux Formula, (MFF), [4], to compute the evolution of shock waves in granular gases, generated by either a vibrating piston under the gravity field or a granular gas accelerated by the gravity field hitting an obstacle at rest. MFF has been widely used in a variety of complex flows, like relativistic flows, [3, 18], stiff reactive terms, [6, 21], real gases, [26], Richtmyer-Meshkov instabilities in two-component compressible flow, [17], and laser imprint instabilities, [20]. In order to implement MFF we need to know the complete spectral decomposition of the Jacobian and the qualitative properties of the associated wave structure. We exhibit the eigenvalues and a complete system of eigenvectors showing the characteristic fields, corresponding to the hyperbolic system of equations for compressible granular flow in one and two spatial dimensions. We have analyzed the thermodynamical variables associated to the granular EOS relevant for the propagation of acoustic waves. Indeed, we have obtained analytical formulas for the adiabatic exponent, the Grüneisen coefficient and the fundamental derivative, showing that none of those variables are constant and the fundamental derivative is strictly positive, (it does not change sign), and, therefore, the nonlinear characteristic fields are genuinely nonlinear with positive nonlinearity, [27]. Thus, we have a simple and consistent formulation of the MFF in terms of the spectral decomposition of the Jacobian, and the above thermodynamical properties show that MFF approximates the unique solution of the Riemann problem correctly. The granular EOS shows that the granular gas becomes less compressible near close-packed limit since the speed of sound tends to infinity when the density tends to that limit for constant granular temperature. We have observed through our numerical experiments, that MFF works robust for low densities, near the close-packed limit and high Mach numbers in inelastic granular gases, and it behaves in agreement with experimental and theoretical studies, [1, 2, 8, 22].

The paper is organized as follows. In Section 2 we settle up our equations and notation, analyzing the spectral decomposition of the Jacobian and the qualitative properties of the waves. In Section 3 we describe the algorithm used, describing the first order Marquina's Flux Formula and the high order accurate extension using either the third-order accurate PHM reconstruction procedure, [16], or the fifth-order accurate Weighted Power ENO recontruction method, [24]. In Section 4 we present several numerical simulations in order to show numerical evidence of the ability and robustness of our algorithm to simulate shock wave propagation in inelastic granular gases. In Section 4.1 we analyze the reflected shock wave generated when a granular gas hits a solid wall under the acceleration of gravity. In Section 4.2 we have computed different time evolution of blast waves in one-dimensional granular gases for different restitution coefficients in the absence of gravity, observing the clustering effect at the contact wave in finite time for the inelastic cases. In Section 4.3 we have computed a one-dimensional vertically vibrated granular layer under sinusoidal perturbations of the gravity, evolving in time. In Section 4.4 we analyze the two-dimensional spectral decomposition of the Jacobians and we address the two-dimensional supersonic granular gas flow hitting a wedge under the gravity field. In Section 5 we draw our conclusions.

2 Euler equations for compressible granular flows

For the sake of understanding we restrict our discussion in this Section to one spatial dimension. The one-dimensional Euler equations for inelastic granular flow can be written as:

$$\begin{aligned}
\rho_t + (\rho u)_x &= 0 \\
(\rho u)_t + \Big(P + \frac{(\rho u)^2}{\rho}\Big)_x &= \rho g \\
E_t + (u(E+P)\ )_x &= -\Theta + \rho g u
\end{aligned}$$

where ρ is the granular gas density, u is the velocity, P is the pressure , Θ is the energy loss term and E is the total granular energy,

$$E = \frac{1}{2}\rho u^2 + \rho\epsilon$$

being ϵ the specific internal energy per unit of volume. We shall use a granular equation of state (EOS) introduced by Goldshtein and Shapiro [7] to compute the pressure, that reads as follows: let σ be the diameter of particles of fixed mass and let e be their restitution coefficient ($0 \leq e \leq 1$). Let $\nu = \frac{\pi}{6}\rho\sigma^3$ be the *volume fraction* being $\nu_{max} = 0.65$ the maximum posible solids volume per unit volume of gas. Then, we have the following expression for the granular EOS:

$$P = (\gamma - 1)\rho A(\rho)\epsilon \tag{1}$$

where γ is the ratio of specific heats for the ideal gas case, (in this paper we use $\gamma = 5/3$), and

$$A(\rho) = 1 + 2(1+e)G(\nu)$$

where,

$$G(\nu) = \nu\Big[1 - \Big(\frac{\nu}{\nu_{max}}\Big)^{\frac{4}{3}\nu_{max}}\Big]^{-1}$$

We define the granular temperature as $T = (\gamma - 1)\epsilon$. Then, we can re-write the granular EOS (1) as

$$P = T\rho A(\rho)$$

On the other hand, the energy loss term acounts for the inelastic collisions, that corresponds to an extension of the so-called *Haff's cooling law*, [11], and it is of the form:

$$\Theta = \frac{12}{\sqrt{\pi}}(1 - e^2)\frac{\rho T^{\frac{3}{2}}}{\sigma}G(\nu) \tag{2}$$

Thus, for the elastic limit $e = 1$ this term has no effect.

We can associate to the granular EOS (1) a well-defined thermodynamic speed of sound, c_s, from the expression:

$$c_s^2 = (\gamma - 1)\epsilon\Big(A(\rho) + \rho A'(\rho) + (\gamma - 1)A^2(\rho)\Big) \tag{3}$$

where

$$A'(\rho) = \frac{\pi}{6}\sigma^3(1+e)\Big(1 + \Big(\frac{4}{3}\nu_{max} - 1\Big)\Big(\frac{\nu}{\nu_{max}}\Big)^{\frac{4}{3}\nu_{max}}\Big)\Big[1 - \Big(\frac{\nu}{\nu_{max}}\Big)^{\frac{4}{3}\nu_{max}}\Big]^{-2}$$

For $0 \leq \nu < \nu_{max}$ it is easy to see that $c_s^2 > 0$ and it is a non negative strictly increasing function of ν, such that $\lim_{\nu \to \nu_{max}} c_s = +\infty$, for constant T. This shows that for *volume fractions* near ν_{max} the granular gas becomes less compressible.

Thus, we can write the eigenvalues and a complete set of eigenvectors of the Jacobian matrix in terms of thermodynamic quantities

$$\begin{aligned} \lambda_1 &= u - c_s \\ \lambda_2 &= u \\ \lambda_3 &= u + c_s \end{aligned}$$

$$\begin{bmatrix} \mathbf{r}_1 & \mathbf{r}_2 & \mathbf{r}_3 \end{bmatrix} = \begin{bmatrix} 1 & 1 & 1 \\ u - c_s & u & u + c_s \\ H - uc_s & H - \frac{1}{b1} & H + uc_s \end{bmatrix}$$

$$\begin{bmatrix} \mathbf{l}_1 \\ \mathbf{l}_2 \\ \mathbf{l}_3 \end{bmatrix} = \begin{bmatrix} \frac{b_2}{2} + \frac{1}{2}\frac{u}{c_s} & -\frac{b_1}{2}u - \frac{1}{2}c_s & \frac{b_1}{2} \\ 1 - b_2 & ub_1 & -b_1 \\ \frac{b_2}{2} - \frac{1}{2}\frac{u}{c_s} & -\frac{b_1}{2}u + \frac{1}{2}c_s & \frac{b_1}{2} \end{bmatrix}$$

where

$$H = \epsilon\Big(1 + (\gamma - 1)A(\rho)\Big) + \frac{1}{2}u^2 \tag{4}$$

is the total enthalpy per unit volume and b_1 and b_2 are defined as:

$$\begin{aligned} b_1 &= (\gamma - 1)\frac{A(\rho)}{c_s^2} \\ b_2 &= 1 + b_1(u^2 - H) \end{aligned}$$

When heat conduction is neglected, as in our case, the properties of the shock waves and rarefaction waves are determined by the adiabatic exponent, the Grüneisen coefficient and the fundamental derivative, [19, 27] that we will define below.

The adiabatic exponent, γ_A, of the granular EOS (1) is defined as

$$\gamma_A := -\frac{V}{P}\frac{\partial P}{\partial V}\bigg|_S \tag{5}$$

where $V = \frac{1}{\rho}$. From the expression

$$\left.\frac{\partial P}{\partial V}\right|_S = -\rho^2 \left.\frac{\partial P}{\partial \rho}\right|_S$$

and the identity $\frac{\partial P}{\partial \rho}|_S = c_s^2$, we have

$$\begin{aligned}
\gamma_A &= \frac{\rho}{P} c_s^2 \\
&= \frac{\rho}{P} T\Big(A(\rho) + \rho A'(\rho) + (\gamma - 1) A^2(\rho)\Big) \\
&= 1 + A(\rho)(\gamma - 1) + \rho \frac{A'(\rho)}{A(\rho)}
\end{aligned}$$

Since $A(\rho) = 1 + 2(1+e)G(\nu)$ we have $\rho A'(\rho) = 2(1+e)\nu G'(\nu)$ and, therefore

$$\gamma_A = \gamma + 2(1+e)\left[G(\nu)(\gamma - 1) + \frac{\nu G'(\nu)}{1 + 2(1+e)G(\nu)}\right] \tag{6}$$

On the other hand, since

$$G(\nu) = \frac{\nu}{1 - \left(\frac{\nu}{\nu_{max}}\right)^{\frac{4}{3}\nu_{max}}}$$

then,

$$G'(\nu) = \frac{1 + \left(\frac{4}{3}\nu_{max} - 1\right)\left(\frac{\nu}{\nu_{max}}\right)^{\frac{4}{3}\nu_{max}}}{\left(1 - \left(\frac{\nu}{\nu_{max}}\right)^{\frac{4}{3}\nu_{max}}\right)^2} \tag{7}$$

therefore,

$$\nu G'(\nu) = G(\nu)\left[1 + \frac{\frac{4}{3}\nu_{max}\left(\frac{\nu}{\nu_{max}}\right)^{\frac{4}{3}\nu_{max}}}{1 - \left(\frac{\nu}{\nu_{max}}\right)^{\frac{4}{3}\nu_{max}}}\right] \tag{8}$$

Thus, we obtain the following expression of the adiabatic exponent in terms of the *volume fraction:*

$$\gamma_A \;=\; \gamma\Big(1+2(1+e)G(\nu)\Big)+\frac{2(1+e)G(\nu)}{1+2(1+e)G(\nu)}\left[\frac{\frac{4}{3}\nu_{max}\left(\frac{\nu}{\nu_{max}}\right)^{\frac{4}{3}\nu_{max}}}{1-\left(\frac{\nu}{\nu_{max}}\right)^{\frac{4}{3}\nu_{max}}}\right] \tag{9}$$

We can easily get an expression of the Grüneisen coefficient also in terms of the *volume fraction*:

$$\begin{aligned}\Gamma &= V\frac{\partial P}{\partial \epsilon}\bigg|_V \\ &= (\gamma-1)(1+2(1+e)G(\nu))\end{aligned} \tag{10}$$

Finally, we are going to get an explicit expression of the fundamental derivative:

$$\begin{aligned}\mathcal{G} &= \frac{1}{2}\frac{V^2}{\gamma_A P}\frac{\partial^2 P}{\partial V^2}\bigg|_S \\ &= \frac{1}{2}\Big[1+\gamma_A-\frac{V}{\gamma_A}\frac{\partial \gamma_A}{\partial V}\Big|_S\Big] \\ &= \frac{1}{2}\Big[1+\gamma_A+\frac{\rho}{\gamma_A}\frac{\partial \gamma_A}{\partial \rho}\Big|_S\Big]\end{aligned} \tag{11}$$

Since $\nu=\frac{\pi}{6}\rho\sigma^3$, we can write $\mathcal{G}$ as

$$\mathcal{G} \;=\; \frac{1}{2}\Big[1+\gamma_A+\frac{\nu}{\gamma_A}\frac{\partial \gamma_A}{\partial \nu}\Big|_S\Big] \tag{12}$$

The following derivative is a straitforward calculation

$$\frac{\partial \gamma_A}{\partial \nu} \;=\; 2(1+e)G'(\nu)\gamma+$$

$$+\frac{2(1+e)\left(\frac{4}{3}\right)^2(\nu_{max})^3\left[\left(\frac{\nu}{\nu_{max}}\right)^{\frac{4}{3}\nu_{max}}+\frac{\nu}{\nu_{max}}\right]}{[1+2(1+e)G(\nu)]\left(1-\left(\frac{\nu}{\nu_{max}}\right)^{\frac{4}{3}\nu_{max}}\right)^3}+$$

$$+\left[\frac{\frac{4}{3}\nu_{max}\left(\frac{\nu}{\nu_{max}}\right)^{\frac{4}{3}\nu_{max}}}{1-\left(\frac{\nu}{\nu_{max}}\right)^{\frac{4}{3}\nu_{max}}}\right]\frac{2(1+e)G'(\nu)}{[1+2(1+e)G(\nu)]^2} \tag{13}$$

and using (9) we have an explicit expression of the fundamental derivative in terms of the *volume fraction*.

In Fig. 1 we display the plots of the adiabatic exponent, the Grüneisen coefficient and the fundamental derivative as functions of the *volume fraction* in the interval $[0, 0.55[$, for two different values of the restitution coefficient $e = 0.9$, 0.2, using 100 points. The profiles of these three thermodynamic quantities are non negative strictly increasing functions of the *volume fraction*, tending to infinity when ν tends to ν_{max} and their minimum values are the corresponding ones for the ideal gas case.

We can recover the ideal gas EOS by putting $\sigma = 0$, and, therefore, these three quantities are constant with respect to the density ρ and their values are $\gamma_A = \gamma$, $\Gamma = \gamma - 1$ and $\mathcal{G} = \frac{1}{2}(1+\gamma)$.

For a granular EOS, $\sigma > 0$, we have the following inequalities:

$$\gamma_A > \gamma, \tag{14}$$

$$\Gamma > \gamma - 1, \tag{15}$$

$$\mathcal{G} > \frac{1}{2}(1+\gamma), \tag{16}$$

for any $\nu > 0$. Thus, the fundamental derivative is always larger than 1, implying that the isentropes in the $P-\rho$ plane are convex, and, since $\Gamma > 0$ the isentropes

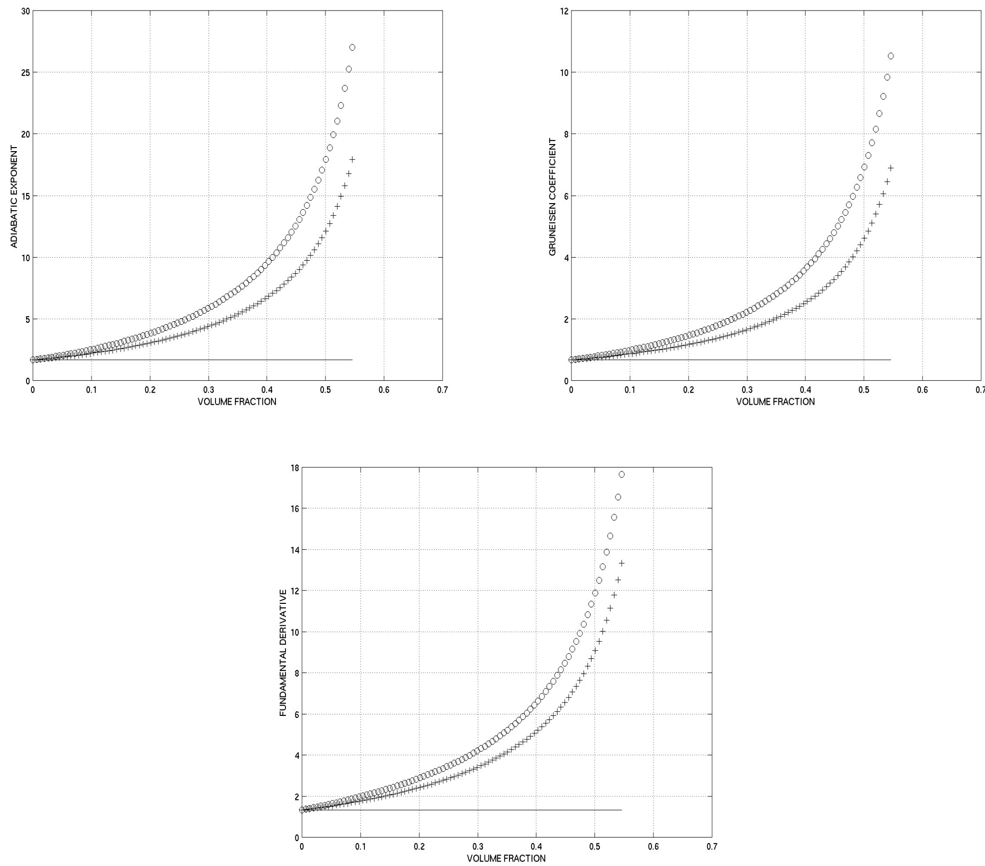

Figure 1: Top left: Volume fraction vs. Adiabatic exponent; top right: Volume fraction vs. Gruneisen coefficient; bottom: Volume fraction vs. Fundamental derivative, e=0.9: 'o'; e=0.2: '+'

do not cross each other in the $P-V$ plane. Thus, the Riemann problem has a unique standard solution, [19]. Indeed, the granular EOS always satisfies the Menikoff-Plohr "strong condition", ([19], p. 95), since

$$\Gamma = PV/\epsilon.$$

When the *volume fraction* is very small the granular gas ressembles an ideal gas, since γ_A, Γ and $\mathcal{G}$, are close to γ, $\gamma-1$ and $\frac{1}{2}(1+\gamma)$, respectively.

We can conclude from the above expressions that the system is strictly hyperbolic and the characteristics fields are either genuinely nonlinear or linear degenerate. The main difference between this model for inelastic granular gas and the Euler equations for ideal gas is in the energy loss term appearing in the energy equation. We will describe the two-dimensional model equations in section 4.

3 An approximate Riemann solver suitable for granular gases

We consider the one-dimensional hyperbolic system of conservation laws

$$\mathbf{u}_t + (\mathbf{f}(\mathbf{u}))_x = 0, \tag{17}$$

together with the initial data

$$\mathbf{u}(x, 0) := \mathbf{u}_0(x), \tag{18}$$

such that the Jacobian matrix $\frac{\partial \mathbf{f}}{\partial t}$ has real eigenvalues $\lambda_p(\mathbf{u}) = 1, ..., m$ and a complete system of eigenvectors $\mathbf{r}^p(\mathbf{u})$, $\mathbf{l}^p(\mathbf{u})$, $p = 1, ..., m$ such that

$$\mathbf{r}^i(\mathbf{u}) \cdot \mathbf{l}^j(\mathbf{u}) = \delta_{ij}$$

and the characteristic fields are either genuinely nonlinear or linear degenerate.

We consider the following computational grid: $x_j = jh$, (h is the spatial step), $t_n = n\Delta t$, is the time discretization, (Δt is the time step), $I_j = [x_{j-\frac{1}{2}}, x_{j+\frac{1}{2}}]$ is the spatial cell, where $x_{j+\frac{1}{2}} = x_j + \frac{h}{2}$ is the cell interface and $C_j^n = [x_{j-\frac{1}{2}}, x_{j+\frac{1}{2}}] \times [t_n, t_{n+1}]$ is the computational cell. Let $\mathbf{u}_j^n$ be an aproximation of the mean value in I_j, $\frac{1}{h}\int_{x_{j-\frac{1}{2}}}^{x_{j+\frac{1}{2}}} \mathbf{u}(x, t_n)dx$, of the exact solution $\mathbf{u}(x, t_n)$ of the initial value problem (17) and (18), obtained from a finite volume scheme in conservation form:

$$\mathbf{u}_j^{n+1} = \mathbf{u}_j^n - \frac{\Delta t}{h}(\tilde{\mathbf{f}}_{j+\frac{1}{2}} - \tilde{\mathbf{f}}_{j-\frac{1}{2}}), \tag{19}$$

where the numerical flux, $\tilde{\mathbf{f}}$, is a function of $k + l$ variables

$$\tilde{\mathbf{f}}_{j+\frac{1}{2}} = \tilde{\mathbf{f}}(\mathbf{u}_{j-k+1}^n, \cdots \mathbf{u}_{j+l}^n), \tag{20}$$

which is consistent with the flux of the equation (17),

$$\tilde{\mathbf{f}}(\mathbf{u}, \cdots, \mathbf{u}) = \mathbf{f}(\mathbf{u}) \tag{21}$$

From the classic theorem of Lax and Wendroff we know that the limit solution of a consistent scheme in conservation form is a weak solution of the hyperbolic PDE system and their discontinuities propagate at the correct speeds. Thus, a consistent scheme in conservation form is the main ingredient to design shock capturing schemes. In order to construct an explicit scheme in conservation form we need a flux formula that approximates the numerical flux $\tilde{\mathbf{f}}$ at every cell interface.

Marquina's Flux Formula, (MFF) [4], computes a consistent numerical flux depending on two neighboring values, $\mathbf{u}_l$ and $\mathbf{u}_r$ by means of the following procedure:

Given the left and right states, $\mathbf{u}_l$ and $\mathbf{u}_r$ we compute the "sided" local characteristic variables

$$\begin{aligned} w_l^p &= \mathbf{l}^p(\mathbf{u}_l) \cdot \mathbf{u}_l \\ w_r^p &= \mathbf{l}^p(\mathbf{u}_r) \cdot \mathbf{u}_r \end{aligned}$$

and the corresponding characteristic fluxes:

$$\begin{aligned} \phi_l^p &= \mathbf{l}^p(\mathbf{u}_l) \cdot \mathbf{f}(\mathbf{u}_l) \\ \phi_r^p &= \mathbf{l}^p(\mathbf{u}_r) \cdot \mathbf{f}(\mathbf{u}_r) \end{aligned}$$

for $p = 1, 2, ..., m$. Let $\lambda_1(\mathbf{u}_l), ..., \lambda_m(\mathbf{u}_l)$, and $\lambda_1(\mathbf{u}_r), ..., \lambda_m(\mathbf{u}_r)$ be their corresponding eigenvalues. We proceed as follows:

If $\lambda_k(\mathbf{u})$ does not change sign in $[\mathbf{u}_l, \mathbf{u}_r]$ then,

if $\lambda_k(\mathbf{u}_l) > 0$ **then**

$\phi_+^k = \phi_l^k$

$\phi_-^k = 0$

else

$\phi_+^k = 0$

$\phi_-^k = \phi_r^k$

end

else

$\alpha^k = \max\{|\lambda_k(\mathbf{u}_l), |\lambda_k(\mathbf{u}_r)|\}$

$\phi_+^k = 0.5(\phi_l^k + \alpha_k w_l^k)$

$\phi_-^k = 0.5(\phi_r^k - \alpha_k w_l^k)$

end

We use the above value of α_k since for our case (granular gas), the local characteristic fields are either linear degenerate or genuinely nonlinear, and this value is a correct prescription of the local viscosity to get an approximate entropy-satisfying solution. Then MFF reads as follows

$$\mathbf{F}^M(\mathbf{u}_l, \mathbf{u}_r) \quad = \quad \sum_{p=1}^{m} \{\phi_+^k \mathbf{r}^p(\mathbf{u}_l) + \phi_-^k \mathbf{r}^p(\mathbf{u}_r)\} \tag{22}$$

where $\mathbf{r}^p(\mathbf{u}_l)$ and $\mathbf{r}^p(\mathbf{u}_r)$ are the right (normalized) eigenvectors of the Jacobian matrices $\frac{\partial \mathbf{f}(\mathbf{u})}{\partial \mathbf{u}}|_{\mathbf{u}=\mathbf{u}_l}$ and $\frac{\partial \mathbf{f}(\mathbf{u})}{\partial \mathbf{u}}|_{\mathbf{u}=\mathbf{u}_r}$, respectively.

Thus, the first order scheme based on MFF is

$$\mathbf{u}_j^{n+1} \quad = \quad \mathbf{u}_j^n - \frac{\Delta t}{h}\Big(\mathbf{F}^M(\mathbf{u}_j^n, \mathbf{u}_{j+1}^n) - \mathbf{F}^M(\mathbf{u}_{j-1}^n, \mathbf{u}_j^n)\Big) \tag{23}$$

The main advantages of MFF are the following:

- It can be applied to nonhomogeneous fluxes, including real gases satisfying thermodynamic consistency, [6], [26].
- The *overheating phenomenon* observed near the piston wall in shock reflection experiments is greately reduced as well as post-shock oscillations, [4], [5].
- MFF scheme behaves robust for low densities, [4].

All the above features are important and desirable to resolve successfully the computations of strong shocks in granular flow, in particular problems concerning blast waves or vibrating pistons.

Higher order of accuracy is obtained by applying a reconstruction procedure on local variables or local fluxes to extrapolate them to the left and right states of the cell interface. In this paper, we have used either the PHM method ([16]) or the fifth-order accurate Weighted PowerENO5 ([24]) and we integrate in time using the third-order accurate Shu-Osher TVD Runge-Kutta time-stepping procedure ([25]).

The calculations were done by using the above mentioned spatial reconstruction procedures applied to each characteristic flux obtained from physical fluxes by local linearizations computed at the interfaces following the so-called Shu-Osher "flux formulation", [25]. Indeed, if q is the charateristic flux we reconstruct $\tilde{q}$ in cell $[x_{j-\frac{1}{2}}, x_{j+\frac{1}{2}}]$ such that

$$q(u(x_j)) = \frac{1}{h}\int_{x_{j-\frac{1}{2}}}^{x_{j+\frac{1}{2}}} \tilde{q}(\xi)d\xi,$$

via primitive function.

For multidimensions, MFF is implemented in a dimension by dimension fashion, where numerical fluxes are computed from physical fluxes in each spatial direction, [4].

4 Numerical Experiments

Our goal is to show numerical evidence that the computational method, described in Section 3, for solving the hydrodynamic model based on the Euler equations for inelastic granular gases, is robust and it allows to examine specific properties of shocks and rarefaction waves related to the energy dissipation term and to explain some experimentally observed processes.

We focus on the following numerical experiments:

- 4.1 Gravity acceleration of granular gases hitting a solid wall until close-packed limit.
- 4.2 Blast waves in granular gases.
- 4.3 One-dimensional vertically vibrated granular layer under gravity acceleration.
- 4.4 Two-dimensional granular gas hitting a wedge under the acceleration of gravity.

In all our calculations we fix the value of the diameter of the particles to be $\sigma = 0.1$. The role of σ in the continuous model is just a scale factor that relates the *volume fraction* and the density appearing in the Euler equations. All the initial data in our numerical experiments are chosen in a way that allows us to examine the behavior of compression and expansion waves in order to check if the resulting physics is consistent.

4.1 Gravity acceleration of granular gas hitting a solid wall until close-packed limit

We consider a one-dimensional domain of length 10 cm., $[0, 10]$, filled with a granular gas at rest with a constant *volume fraction* and a constant pressure distribution with a solid wall at the right end, (i.e., reflective boundary conditions are applied), under the action of the gravity field oriented from left to right. When evolving in time, the granular gas is accelerated by the gravity and it falls towards the right end. As soon as the velocity reaches a supersonic value, a shock wave is formed at the solid wall and propagates to the left. The granular gas starts to cluster near the wall until reaches the close-packed limit.

We start with the following initial data:

$(\rho, v, P) = (34.3774677, 18, 1589.2685472)$, $g = 980\,\mathrm{cm/s}^2$ and restitution coefficient $e = 0.97$.

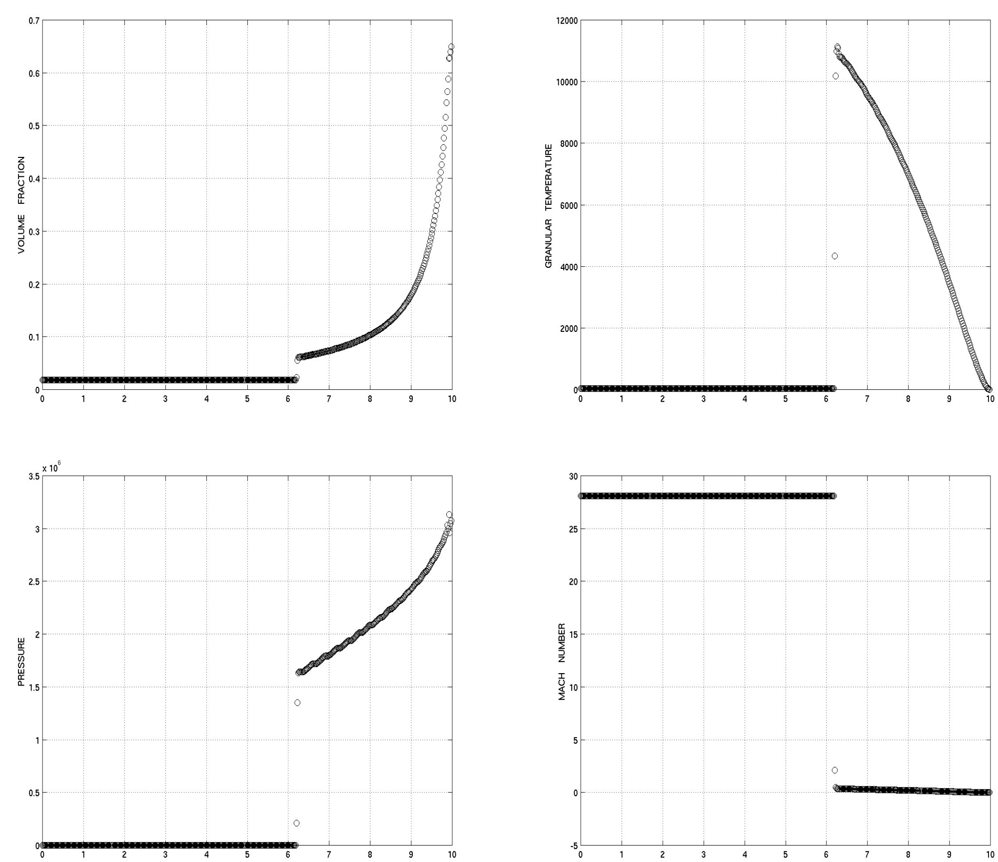

Figure 2: e=0.97, MFF-PHM scheme, top left: *volume fraction*; top right: granular temperature; bottom left: pressure, bottom right: Mach number

We have performed our computation using 1000 grid points, until time 0.23 with a Courant-Friedrichs-Lewy, (CFL), factor of 0.5 using our MFF scheme with the third-order accurate PHM reconstruction. In Fig. 2 we display the *volume fraction*, the granular temperature, the pressure and the Mach number at time 0.23. We observe the rarefaction wave generated by the energy dissipation term where granular temperature becomes close to zero near the wall. We reach at the wall the *volume fraction* 0.649472, near to the close-packed limit 0.65. The reflected shock wave becomes *slowly moving* with respect of the Courant time used in the computation, thus, it generates post-shock oscillations, as it can be observed in the pressure profile.

4.2 Blast waves in granular gases

We consider one-dimensional blast waves generated when evolving in time a Riemann problem where the left state is a supersonic granular gas and the right state is a granular gas at rest, in the absence of gravity. We computed several initial data generating a shock-contact-shock structure. First, we have performed four numerical experiments with restitution coefficients $e = 1$, $e = 0.9$, $e = 0.7$ and $e = 0.2$, using the following initial data, consisting of two constant states, left and right, in the computational domain $[0, 10]$:

$$
\begin{aligned}
(\rho_L, v_L, P_L) &= (44.5, 0.698, 3.528) \\
(\rho_R, v_R, P_R) &= (50, 0, 0.571)
\end{aligned}
$$

where the jump is located at $x = 5$. We have used in our computation 1000 grid points. We evolve until time 5.48 with a CFL factor of 0.1 and the fifth-order accurate Weighted Power ENO5 method, in order to get better resolution of the contact wave, except for the elastic case, ($e = 1$), where we have used the PHM reconstruction to reduce the post-shock oscillations generated behind the shock wave at the left of the contact. When evolving in time we observe the clustering of granular gas around the contact for the inelastic cases. In fact, near the contact wave the gas becomes less compressible and the granular temperature which is high at the shock waves decreases close to zero near the contact when the clustering approaches to the close-packed limit, as predicted by the physics of the inelastic granular gas. We observed that the smaller the restitution is, the faster the clustering (near the contact) approaches to the close-packed limit. We display in Figs. 3 and 4, zoomed regions of the *volume fraction* and granular temperature obtained at time 5.48, from top to bottom corresponding to restitution coefficients $e = 1$, $e = 0.9$, $e = 0.7$ and $e = 0.2$, where we see no clustering for the elastic case and we can observe an increasing degree of clustering near the contact wave for the successive decreasing values of the restitution coefficient. The close-packed limit is always reached in finite time when the restitution coefficient $e < 1$, in spite the initial data consists of low *volume fraction* values.

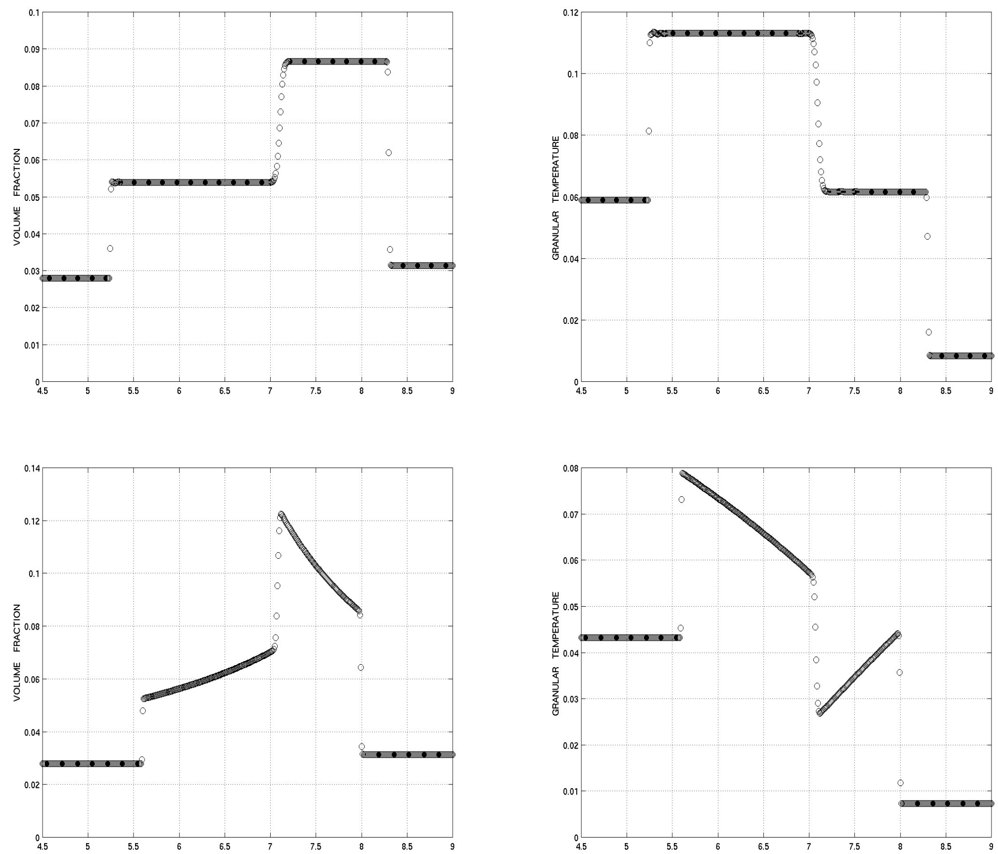

Figure 3: Top: e=1, MFF-PHM scheme, top left: zoomed region of *volume fraction*, top right: zoomed region of granular temperature. Bottom: e=0.9, MFF-Weighted Power ENO5 scheme, bottom left: zoomed region of *volume fraction*, bottom right: zoomed region of granular temperature

The above remarks are still valid for a blast wave experiment evolving through a dense granular gas. We consider the following initial data with $e = 0.9$ and 2000 grid points:

$$\begin{aligned}(\rho_L, v_L, P_L) &= (178, 0.698, 3.528)\\ (\rho_R, v_R, P_R) &= (200, 0, 0.571)\end{aligned}$$

where the jump is located at $x = 2$.

We have computed, using MFF with our fifth-order accurate Weighted Power ENO5 scheme, until time 12 with a CFL factor of 0.1, where the clustering

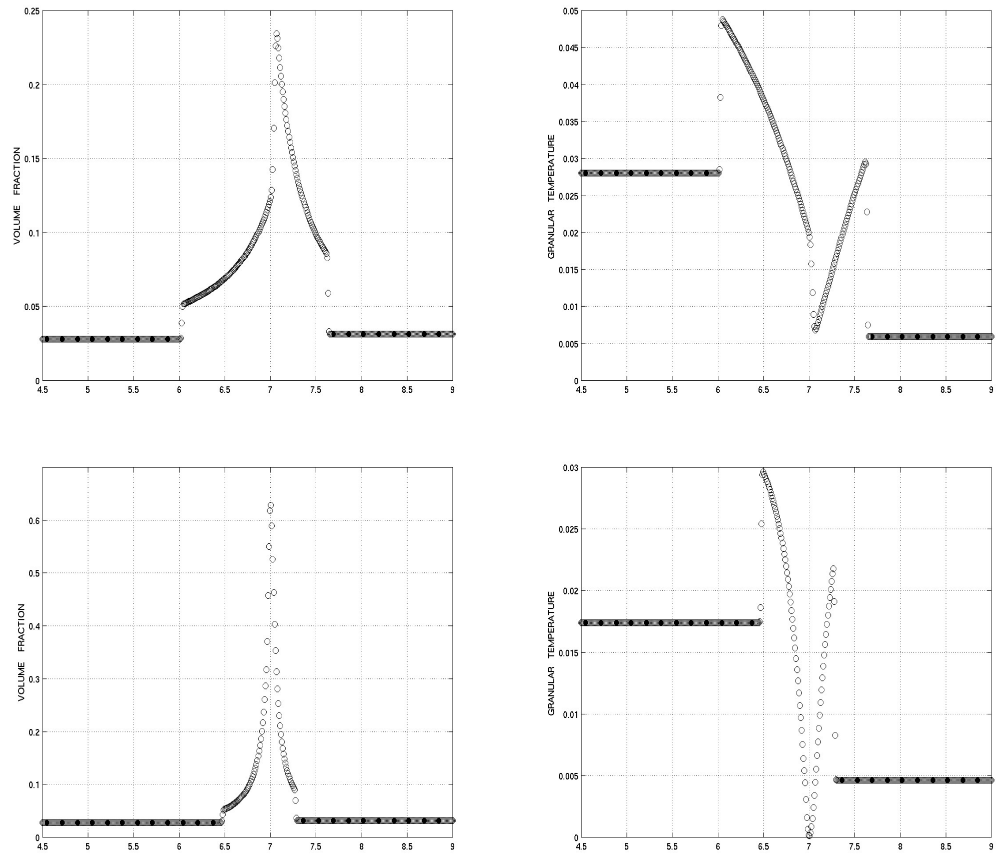

Figure 4: Top: e=0.7, MFF-Weighted Power ENO5 scheme, top left: zoomed region of *volume fraction*, top right: zoomed region of granular temperature; Bottom: e=0.2, MFF-Weighted Power ENO5 scheme, bottom left: zoomed region of*volume fraction*, bottom right: zoomed region of granular temperature

near the contact is very close to the close-packed limit. We display in Fig. 5 zoomed regions of the *volume fraction*, granular temperature and acoustic impedance, ρc_s, where we can still see the contact wave and we can observe that the clustering is stronger at the right side of the contact since the gas is more compressed.

We point out that numerical viscosity associated to the chosen grid, the order of accuracy and the numerical scheme determine the time when close-packed limit is reached along the evolution.

We also remark from the above numerical experiments that blast waves in inelastic granular gases with zero gravity produce clustering around the contact wave, approaching to the close-packed limit in finite time. The above clustering is *dynamic* in the sense that the high density region near the contact wave moves with the flow velocity. Roughly speaking it can be said that when a region of particles is compressed by an acoustic wave, the density and the number of collisions increase, and, therefore, the particles lose energy and are unable to quit this dense region.

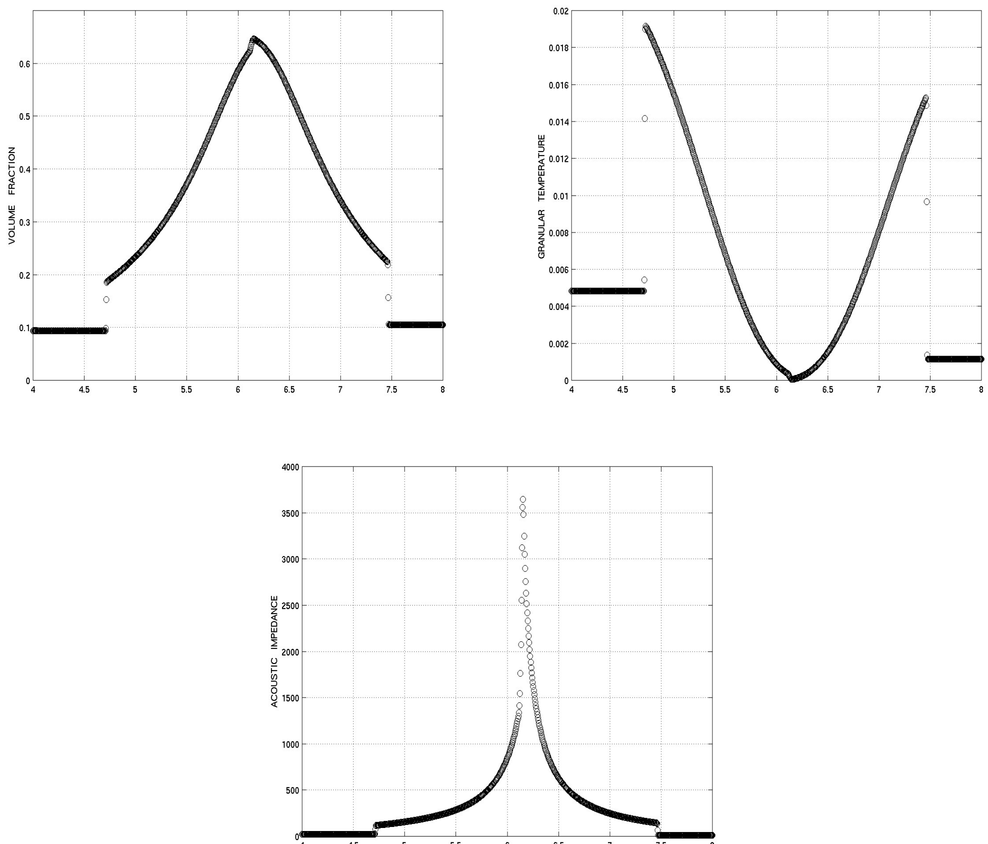

Figure 5: Dense granular gas: e=0.9, MFF-Weighted Power ENO5 scheme, top left: zoomed region of *volume fraction*, top right: zoomed region of granular temperature, botton: zoomed region of acoustic impedance

4.3 One-dimensional vertically vibrated granular layer under gravity acceleration

We consider the one dimensional domain $[0, 0.15]$. The right end (bottom plate) is a solid wall, (i.e. reflective boundary conditions are applied) and the left end (top) is open (i.e. we use inflow/outflow boundary conditions). We assume the action of the acceleration of gravity, $g = 980\,\mathrm{cm/s^2}$, from the top to the bottom plate. We consider the domain filled with a granular gas with restitution coefficient $e = 0.9$, constant granular temperature $T_0 = 1$ and a *volume fraction* distribution profile representing a very low density along the whole domain except at a layer of approximately 0.005 of thickness, defined from the function

$$\eta(x) = \exp(-3000 * x^2),$$

using the formula

$$\nu(x) = \epsilon + \nu_0 \cdot \eta(0.145 - x),$$

for $x \leq 0.145$ and

$$\nu(x) = \epsilon + \nu_0,$$

for $x > 0.145$ where $\epsilon = h$, being h the spatial stepsize.

The *volume fraction* of the layer in the initial profile is chosen to be $\nu_0 = 0.2 \cdot \nu_{max}$, i.e. 20% of the close-packed limit. We compute the initial density, pressure and energy from the above *volume fraction* profile and constant granular temperature, $T_0 = 1$.

We assume the system is vibrating sinusoidally (in the direction of gravity) with amplitude $A > 0$ and frequency f, by using the term $g(1 + A\cos(2\pi f t))$ instead of g in the model. Thus, we start our time evolution when the maximum acceleration of the perturbation of the gravity field occurs. In order to reproduce the compression-expansion wave pattern of a vertically vibrated layer of inelastic granular gas along the evolution in time, we have chosen the values: $A = 3$ and $f = 200$.

We have used a uniform grid of 1500 grid points, a CFL factor of 0.5 and MFF-Weighted Power ENO5 scheme. We evolve in time completing five cycles. In Fig. 6 we display the zoomed profiles of the *volume fraction* (left) and granular temperature (right) for the following successive times, from top to bottom, $f \cdot t = 0.35$, $f \cdot t = 1.35$, $f \cdot t = 2.35$, $f \cdot t = 3.35$, $f \cdot t = 4.35$, where we can see the shock waves and expansion waves propagating along the layer, reproducing the physical mechanism of transformation of the vibrated kinetic energy into granular temperature. We also observe the convergence to a periodic pattern at the fourth and fifth cycle, as we can see in Fig. 7 where we also display the zoomed region of the velocity profile for these two cycles. We have computed the total *volume fraction* at every time step and we have obtained the following values corresponding to the above successive times 28.23, 28.31, 28.28, 28.32 and 28.27, respectively. Since we used inflow/outflow boundary conditions applied at this end, we can conclude that there is no significant mass gain/loss through the left end (top) of our domain along the time evolution.

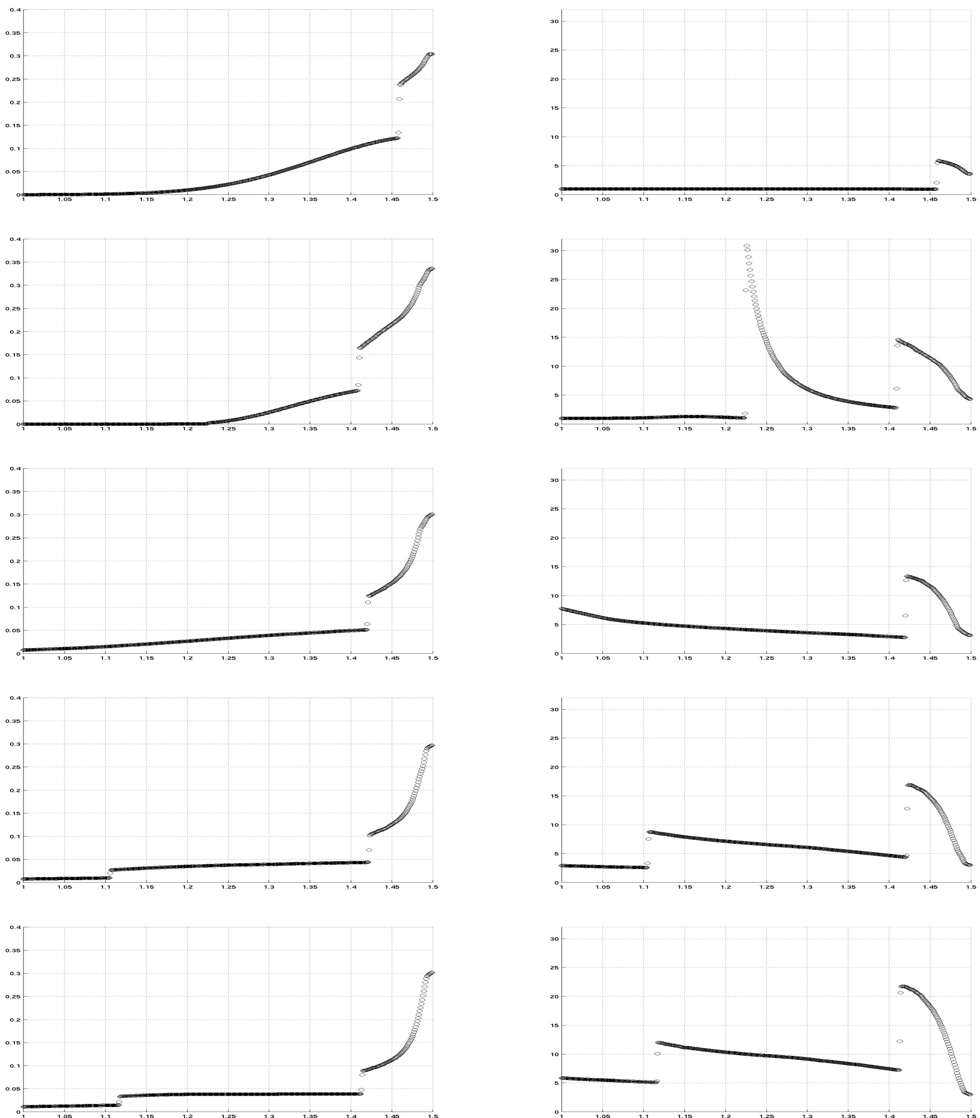

Figure 6: e=0.9, MFF-Weighted Power ENO5 scheme, left: zoomed region of *volume fraction*; right: zoomed region of granular temperature for five cycles at times t where $f \cdot t = 0.35$, 1.35, 2.35, 3.35, 4.35, from top to bottom; abcisas in the pictures are re-scaled using a factor of 10.

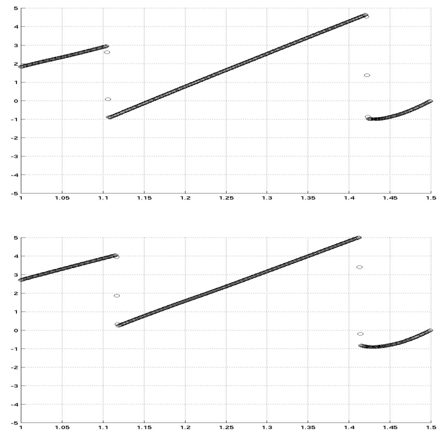

Figure 7: e=0.9, MFF-Weighted Power ENO5 scheme, velocity profiles at $f \cdot t =$ 3.15, 4.15; abcisas in the pictures are re-scaled using a factor of 10.

4.4 Two-dimensional granular gas hitting a wedge under the acceleration of gravity

In two spatial dimensions, the Euler equations for granular gases with energy loss term and gravity acceleration in the direction of the unit vector $(\cos\theta, \sin\theta)$, $\cos^2\theta + \sin^2\theta = 1$, read as follows:

$$\rho_t + (\rho u)_x + (\rho v)_y \quad = \quad 0 \tag{24}$$

$$(\rho u)_t + \Big(P + \frac{(\rho u)^2}{\rho}\Big)_x + (\rho u v)_y \quad = \quad \rho\, g\, \cos\theta \tag{25}$$

$$(\rho v)_t + (\rho u v)_x + \Big(P + \frac{(\rho v)^2}{\rho}\Big)_y \quad = \quad \rho\, g\, \sin\theta \tag{26}$$

$$E_t + (u(E+P)\ )_x + (v(E+P)\ )_y \quad = \quad -\Theta + \rho\, g\,(u\cos\theta + v\sin\theta) \tag{27}$$

where (u, v) is the velocity field, $E = \frac{1}{2}\rho(u^2+v^2) + \rho\epsilon$ is the total energy, P is the pressure computed using the granular EOS (1), and the energy loss term Θ given by (2).

The system ((24)-(27)) is hyperbolic using the well-defined speed of sound (3), where the eigenvalues of the Jacobian of the flux $\mathbf{f}$ in the x-direction, $\frac{\partial \mathbf{f}(\mathbf{u})}{\partial \mathbf{u}}$, are $\lambda_1 = u - c_s$, $\lambda_2 = u$, $\lambda_3 = u$, $\lambda_4 = u + c_s$, and the eigenvalues of the Jacobian of the flux $\mathbf{g}$ in the y-direction, $\frac{\partial \mathbf{g}(\mathbf{u})}{\partial \mathbf{u}}$, are $\mu_1 = v - c_s$, $\mu_2 = v$, $\mu_3 = v$, $\mu_4 = v + c_s$. The Jacobians also have a complete set of eigenvectors,

$$\mathbf{R}^f = \begin{bmatrix} \mathbf{r}_1 & \mathbf{r}_2 & \mathbf{r}_3 & \mathbf{r}_4 \end{bmatrix} = \begin{bmatrix} 1 & 1 & 0 & 1 \\ u - c_s & u & 0 & u + c_s \\ v & v & 1 & v \\ H - uc_s & H - \frac{1}{b_1} & v & H + uc_s \end{bmatrix}$$

$$\mathbf{L}^f = \begin{bmatrix} \mathbf{l}_1 \\ \mathbf{l}_2 \\ \mathbf{l}_3 \\ \mathbf{l}_4 \end{bmatrix} = \begin{bmatrix} \frac{b_2}{2} + \frac{u}{2c_s} & -\frac{b_1 u}{2} - \frac{1}{2c_s} & -\frac{b_1 v}{2} & \frac{b_1}{2} \\ 1 - b_2 & ub_1 & vb_1 & -b_1 \\ -v & 0 & 1 & 0 \\ \frac{b_2}{2} - \frac{u}{2c_s} & -\frac{b_1 u}{2} + \frac{1}{2c_s} & -\frac{b_1 v}{2} & \frac{b_1}{2} \end{bmatrix}$$

where

$$H = \epsilon\Big(1 + (\gamma - 1)A(\rho)\Big) + \frac{1}{2}(u^2 + v^2) \tag{28}$$

is the total enthalpy per unit volume and b_1 and b_2 are defined as:

$$b_1 = (\gamma - 1)\frac{A(\rho)}{c_s^2}$$

$$b_2 = 1 + b_1(u^2 + v^2 - H)$$

The eigenvectors of the Jacobian in the y-direction, $\frac{\partial \mathbf{g}(\mathbf{u})}{\partial \mathbf{u}}$, are obtained by changing the roles of u and v and the second and third components of each left and right eigenvector.

Our computational domain is a square of side 10 cm. This domain contains a step which is a square of side 5 cm. located at the bottom right of the domain. Reflective boundary conditions are applied along the inner sides of the step. Inflow boundary conditions are applied at the left-hand end and the upper end of the domain and outflow boundary conditions are applied at the upper right end and the bottom left end of the domain. We fill the domain with a granular gas with an initial speed of sound of 9 cm/s. We have performed two numerical experiments, using two possible *volume fractions*, $\nu_{1i} = 0.018$ (low dense granular gas) and $\nu_{2i} = 0.18$ (dense granular gas). In both cases, the initial

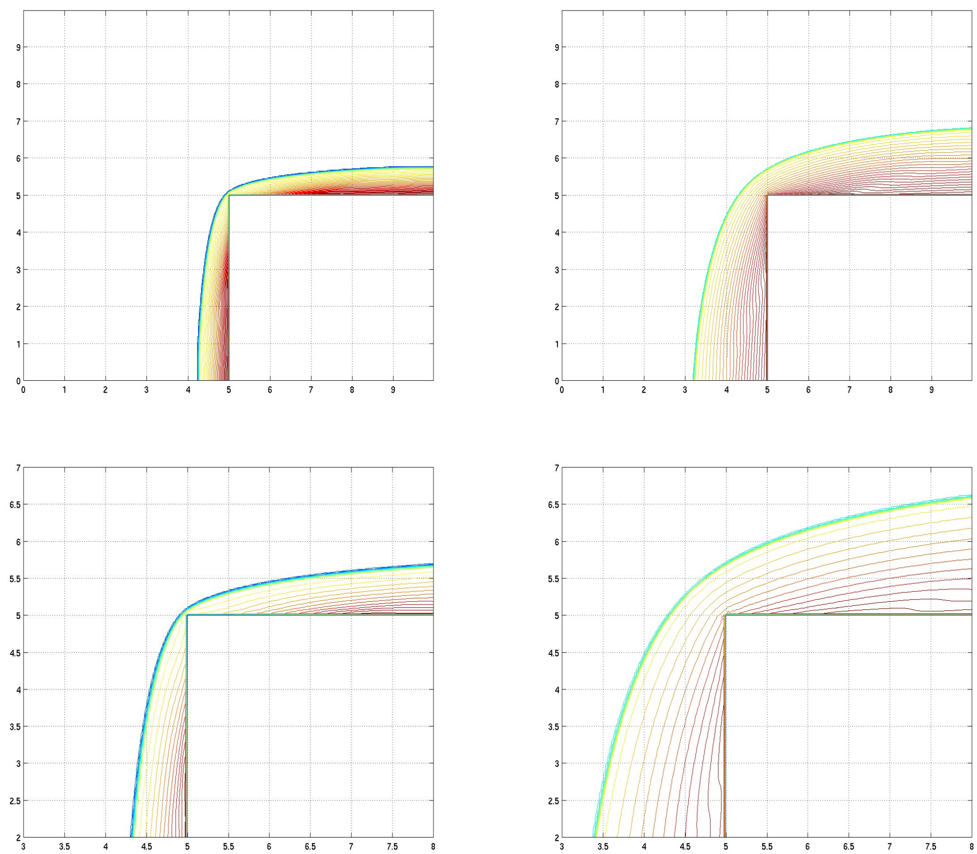

Figure 8: e=0.97, MFF-PHM scheme, top left: *volume fraction* contour lines of the low dense granular gas experiment; top right: *volume fraction* contour lines of the dense granular gas experiment; bottom: corresponding zoomed regions near the corner

velocity field (u_i, v_i) is established in the direction $\theta = -45^o$ with an initial Mach number of 7, and the acceleration of gravity $g = 980\,\mathrm{cm/s}^2$ is applied following the same direction and orientation. We have used the restitution coefficient $e = 0.97$. We point out that the initial data corresponding to the first experiment, (low dense granular gas), were taken from [23]. We have computed density, moment and total energy from the above initial conditions, using the expression of the speed of sound (3). Indeed, our initial data for both experiments are

$$(\rho_{1i}, u_{1i}, v_{1i}, P_{1i}) = (34.3774677, 44.547727, -44.547727, 1589.2685472),$$

and

$$(\rho_{2i}, u_{2i}, v_{2i}, P_{2i}) = (343.7746770, 44.547727, -44.547727, 10174.873548),$$

respectively.

We evolve in time both initial data, using our MFF-PHM scheme, for a uniform grid of 400x400 grid points until the flow reaches a Mach number of 12 and 15.5, respectively. The granular gas hits the wedge and a reflective shock wave is generated. After the shock the flow has a higher *volume fraction* and higher granular temperature and the maximum *volume fraction* reached are $\nu_1^m = 0.1033$ at time 0.0425 for the low dense granular gas experiment, and $\nu_2^m = 0.5177$ at time 0.0412 for the second one. In Fig. 8 we display the *volume fraction* contour lines corresponding to both experiments at the times indicated above, (top left and right, respectively) and the corresponding zoomed regions near the corner, (bottom left and right, respectively). We did not found significant differences by using our fifth-order accurate scheme instead of PHM, since only shock waves are involved in these experiments.

5 Conclusions

In this paper we have implemented a robust approximate Riemann solver to approximate the evolution of shock waves in inelastic granular gases, modeled by means of the Euler equations together with an equation of state that represents the fluidized granular gas until the close-packed limit, and an energy dissipation term accounting for the energy loss by inelastic collisions of particles. We have observed through our numerical experiments that blast waves propagating in inelastic granular gases cluster at the contact wave until close-packed limit in finite time. We also observed that our algorithm is able to transform the kinetic energy applied on a vibrated granular layer into granular temperature under the gravity field. We also computed a two dimensional supersonic granular flow hitting a wedge under the action of gravity field. In spite we are not intending to reproduce observed experimental data in this paper, we have shown that our numerical method together with the model used behave in agreement with the physics of the fluidized inelastic granular gas. Additional numerical experiments in two dimensional inelastic granular gases are the object of future work.

6 Acknowledgements

The authors thank José Antonio Carrillo for insightful discussions and valuable references on kinetic and hydrodynamic models for granular media.

The second author acknowledges support from “Secretaria de Estado de Educación y Universidades” of the Spanish government, through a “Beca de Estancia en el Extranjero del Programa Salvador de Madariaga”.

This research was carry out while the authors were visiting UCLA Department of Mathematics and they are very grateful to the people of the Computational and Applied Mathematics research group for their hospitality.

References

[1] K. M. Aoki and T. Akiyama, Simulation studies of pressure and density wave propagations in vertically vibrated beds of granules, Phys. Rev. E 52 (1995) 3288–3291.

[2] J. Bougie, Sung Joon Moon, J. B. Swift and H. L. Swinney, Shocks in vertically oscillated granular layers, Phys. Rev. E 66 (2002) 051301.

[3] R. Donat, J.A. Font, J.M. Ibañez and A. Marquina, A flux-split algorithm applied to relativistic flows, J. Comput. Phys. 146 (1998) 58–81.

[4] R. Donat and A. Marquina, Capturing Shock Reflections: An improved Flux Formula, J. Comput. Phys. 125 (1996) 42–58.

[5] R. Fedkiw, A. Marquina and B. Merriman, An isobaric fix for the overheating problem in multimaterial compressible flows, J. Comput. Phys. 148 (1999) 545–578.

[6] R. Fedkiw, B. Merriman, R. Donat and S. J. Osher, The penultimate scheme for systems of conservation laws: finite difference ENO with Marquina's flux splitting, In Hafez, M.M. and Chattot, J.J. (eds), Innovative Methods for Numerical Solutions of PDEs (1997) 49–85.

[7] A. Goldshtein and M. Shapiro, Mechanics of collisional motion of granular materials: Part 1. General hydrodynamic equations, J. Fluid Mech. 282 (1995) 75–114.

[8] A. Goldshtein, M. Shapiro, L. Moldavsky and M. Fishman, Mechanics of collisional motion of granular materials: Part 2. Wave propagation through a granular layer, J. Fluid Mech. 287 (1995) 349–382.

[9] A. Goldshtein, M. Shapiro and C. Gutfinger, Mechanics of collisional motion of granular materials: Part 3. Self-similar shock wave propagation, J. Fluid Mech. 316 (1996) 29–51.

[10] A. Goldshtein, M. Shapiro and C. Gutfinger, Mechanics of collisional motion of granular materials: Part 4. Expansion wave, J. Fluid Mech. 327 (1996) 117–138.

[11] P.K. Haff, Grain flow as a fluid-mechanical phenomenon , J. Fluid Mech. 134 (1983) 401–430.

[12] J. T. Jenkins and M. W. Richman, Grad 13-moment system for a dense gas of inelastic spheres, Arch. Ration. Mech. Anal. 87 (1983) 355–377.

[13] V. Kamenetsky, A. Goldshtein, M. Shapiro and D. Degani, Evolution of a shock wave in a granular gas, Phys. of Fluids 12 (2000) 3036–3049.

[14] A. Kudrolli, M. Wolpert and J. P. Gollub, Cluster formation due to collision in granular gases, Phys. Rev. Lett. 78 (1996) 1383–1386.

[15] C. K. K. Lun, S. B. Savage, D. J. Jeffrey and N. Chepurny, Kinetic theories of granular flow: Inelastic particles in Couette flow and slightly inelastic particles in a general flow field, J. Fluid Mech. 140 (1984) 223–256.

[16] A. Marquina, Local Piecewise Hyperbolic Reconstructions for Nonlinear Scalar Conservation Laws, SIAM J. Sci. Comp. 15 (1994) 892–915.

[17] A. Marquina and P. Mulet, A flux-split algorithm applied to conservative models for multicomponent compressible flows, J. Comput. Phys. 185 (2003) 120–138.

[18] J. M. Martí, E. Muller, J.A. Font, J.M. Ibáñez and A. Marquina, Morphology and dynamics of relativistic jets, Astrophys. J. 479 (1997) 151.

[19] R. Menikoff and B.J. Plohr, The Riemann problem for fluid flow of real materials, Rev. Mod. Phys. 61 (1989) 75-130.

[20] N. Ohnishi, H Nagatomo, H Nishimura, H Takabe and T. Yamanaka, Radiation effects on hydrodynamic perturbation growth due to non-uniform laser irradiation, J. Quant. Spectrosc. Ra. 71 (2001) 551–560.

[21] S. J. Osher, R. P. Fedkiw, Level Set Methods and Dynamic Implicit Surfaces, Springer-Verlag, New York, 2002.

[22] A. V. Potatov and C. Campbell, Propagation of inelastic waves in deep vertically shaken particle beds, Phys. Rev. Lett. 77 (1996) 4760–4763.

[23] E. C. Rericha, C. Bizon, M.D. Shattuck and H. L. Swinney, Shocks in Supersonic Sand, Phys. Rev. Lett. 88 (2002) 014302.

[24] S. Serna and A. Marquina, Power ENO methods: A fifth-order accurate Weighted Power ENO method, J. Comput. Phys. (2004), (in press), http://dx. doi.org/10.1016/j.jcp.2003.09.017

[25] C. W. Shu and S. J. Osher, Efficient Implementation of Essentially Non-Oscillatory Shock Capturing Schemes II, J. Comput. Phys. 83 (1989) 32–78.

[26] Y. Stiriba, A. Marquina and R. Donat, Equilibrium real gas computations using Marquina's scheme, Int. J. Numer. Methods in Fluids 41 (2003) 275–301.

[27] P. Thompson, A Fundamental Derivative of Gas Dynamics, Phys. Fluids 14 (1971) 1843–1849.